Available online at www.sciencedirect.com

ScienceDirect

Advances in Space Research 66 (2020) 243–258

ADVANCES IN SPACE RESEARCH (a COSPAR publication)

www.elsevier.com/locate/asr

Maximum usable frequency and skip distance maps over Italy

M. Pietrella *, M. Pezzopane

Istituto Nazionale di Geofisica e Vulcanologia, Via di Vigna Murata 605, 00143 Roma, Italy

Received 9 December 2019; received in revised form 19 February 2020; accepted 28 March 2020
Available online 9 April 2020

Abstract

Since 1988 the Upper Atmosphere Physics unit of the Istituto Nazionale di Geofisica e Vulcanologia (INGV) has provided maps of Maximum Usable Frequency (*MUF*) and *skip distance* over a European area extending in latitude from 34°N to 60°N and in longitude from 5°W to 40°E. Anyhow, these maps suffer the following restrictions: (1) they are provided with two months in advance and so they are not suitable for space weather purposes; (2) they are represented with few isolines; (3) they are centred only on Rome (41.8°N, 12.5°E) and generated in black and white; (4) *MUF* are calculated with a really simple algorithm. In order to overcome these restrictions, a new software tool was developed to get climatological maps (up to three months in advance) and quasi real-time maps, (nowcasting) limited to the sector extending in latitude from 34°N to 48°N and in longitude from 5°E to 20°E, which includes the whole Italian territory. In order to achieve a greater accuracy, *MUF* and *skip distance* maps are generated combining the Simplified Ionospheric Regional Model (SIRM) and its UPdated version (SIRMUP) with the Lockwood algorithm. Climatological maps are generated every hour on the basis of the predicted 12-months smoothed sunspots number. Nowcasting maps are generated every 15 min exploiting *fo*F2 and *M*(3000)F2 data autoscaled at the ionospheric stations of Rome and Gibilmanna (37.6°N, 14.0°E). Nowcasting maps constitute the most important novelty because they let High Frequency (HF) users know in quasi real-time the radio propagation conditions over Italy. This turns out to be very valuable in terms of reliable radio links, especially in case of adverse space weather events.

Keywords: Maximum usable frequency; Skip distance; Lockwood formula; SIRM

1. Introduction

The term space weather generally refers to conditions on the Sun, in the solar wind, and within Earth's magnetosphere, ionosphere and thermosphere that can influence the performance and reliability of space-borne and ground-based technological systems. Specifically, the Sun emits energy as flares of electromagnetic radiation (from radio waves to X-rays), and as energetic electrically charged particles through coronal mass ejections and plasma streams. The electromagnetic radiation travels at the speed of light and takes about eight minutes to move from Sun to Earth, whereas the charged particles travel more slowly, taking from a few hours to several days. Radiation, particles and interplanetary magnetic field interact with the Earth's geomagnetic field and outer atmosphere in complex ways, triggering, under specific conditions, geomagnetic and ionospheric storms, auroras and a number of effects that, depending on their intensity, can cause disruptions to Global Position System (GPS) navigation, failure or misoperation of satellites, thus endangering human life or health.

The High Frequency (HF, 3–30 MHz) point-to-point communications rely on the ionosphere to propagate radio signals, and they are a valuable alternative and complement to satellite communications. In particular, the ionosphere is a dynamic propagation environment and this makes HF communications challenging during space

* Corresponding author.
E-mail addresses: marco.pietrella@ingv.it (M. Pietrella), michael.pezzopane@ingv.it (M. Pezzopane).

https://doi.org/10.1016/j.asr.2020.03.040
0273-1177/

weather events, when the ionosphere deviates substantially with respect to its median behaviour. In such circumstances, the effects on the radio systems may be prompt (i.e. they occur soon after the initial event on the Sun) or delayed (i.e. they occur some days later) and generally during ionospheric storms regional and global reductions in the operational HF band occur. In these situations successful HF communications may depend on timely and accurate information on ionospheric radio propagation conditions.

To this regard, thanks to the modern ionospheric stations, equipped with ionograms automatic scaling software such as the Automatic Real-Time Ionogram Scaler with True height analysis (ARTIST) (Reinisch and Huang 1983; Reinisch et al. 2005; Galkin and Reinisch 2008) and Autoscala (Scotto and Pezzopane 2002, 2008; Pezzopane and Scotto 2005, 2007; Scotto 2009; Scotto et al. 2012), and real-time data transmission, it is possible to minimise the degradation of HF services, thus maximising their reliability.

Positive and negative phases can be observed in the ionospheric plasma during magneto-ionospheric storms. In these circumstances, climatological values are dramatically different from real ones. For instance, during a negative ionospheric phase (i.e. real values lower than climatological ones) the Maximum Usable Frequency (*MUF*) that can be used to perform a radio link is by far lower than that normally working in case of quiet ionosphere; in this case, a frequency transmitted around the climatological value would pass through the ionosphere, being never reflected. This means that although climatological global models, such as the International Reference Ionosphere (IRI) model (Bilitza and Reinisch, 2008; Bilitza et al., 2014, 2017) and NeQuick (e.g. Radicella, 2009), give a valid representation of the quiet ionosphere, their use to calculate the critical frequency of the F2 ionospheric layer associated to the ordinary mode of propagation (*fo*F2) and the propagation factor (*M*(3000)F2), in case of disturbed ionosphere would not be reliable at all, and so corresponding *MUF* values and radio links. That is why systematic investigations were undertaken to study and develop methods and services in order to mitigate the ionospheric impact on HF communication systems during important space weather events.

Just for space weather purposes, since 2006, in the framework of the DIAS (DIgital upper Atmosphere Server) project (Belehaki et al., 2005), nowcasting *fo*F2 and *M*(3000)F2 maps have been generated over the mid-latitude European area on the base of the Simplified Ionospheric Regional Model Updated (SIRMUP) (Zolesi et al., 2004; Tsagouri et al., 2005). More recently, in the framework of the Space Situational Awareness (SSA) Programme P2-SWE-1 (http://swe.ssa.esa.int/web/) (Belehaki et al., 2015), *fo*F2 nowcasting maps were extended to polar areas (Pietrella, 2015); in addition, *fo*F2 forecasting maps based on the Solar Wind driven autoregression model for Ionospheric short-term Forecast (SWIF) (Tsagouri and Belehaki, 2008; Tsagouri et al. 2009) have been also generated. Both products are available through the DIAS portal (*http://www.iono.noa.gr/DIAS/*).

Among the other products offered by the DIAS system for space weather purposes, of particular importance are also the *MUF* and *skip distance* nowcasting maps covering the European area extending in longitude from 5°W to 40° E and in latitude from 34°N to 60°N. They are generated on the base of *fo*F2 and *M*(3000)F2 predictions provided by the SIRMUP model and the Lockwood's (LKW) algorithm (Lockwood, 1983).

Since 1988 the Upper Atmosphere Physics unit of the Istituto Nazionale di Geofisica e Vulcanologia (INGV) has provided *MUF* and *skip distance* climatological maps with two months in advance over the same area considered in the DIAS system. If one would establish a radio link over the Italian region, the use of these maps is not straightforward because of some limitations: (1) since these are long-term prediction maps, they are not appropriate for space weather purposes; (2) *MUF* are calculated with a simpler algorithm than the one by Lockwood (1983); (3) maps are generated with few isolines, and consequently a detailed description of the *MUF* and *skip distance* over Italy is missing; (4) they are centred only on Rome (considered as the transmitting point) and output in black and white.

To overcome these restrictions a new software tool was developed, generating *MUF* and *skip distance* climatological and nowcasting maps in a more restricted area extending in latitude from 34°N to 48°N and in longitude from 5° E to 20°E, including the whole Italian territory. In particular, coloured maps no longer centred only on Rome but also on additional three transmitting points, i.e. Milan (45.5°N; 9.2°E), Cagliari (39.2°N; 9.1°E), and Catania (37.5°N; 15.1°E), located in the Northern, Western, and Southern part of Italy respectively, are generated with an increased number of isolines. This guarantees a much more reliable coverage of the Italian area, especially for disturbed conditions when the ionospheric plasma may be characterized by small scale irregularities. It is noteworthy that *MUF* and *skip distance* maps are generated using for the first time over Italy the algorithm developed by Lockwood (1983), which guarantees a greater accuracy for the *MUF* calculation.

Specifically, *MUF* and *skip distance* climatological maps up to three months in advance are produced applying the SIRM&LKW procedure (Zolesi et al., 2008) that is a combination of the Simplified Ionospheric Regional Model (SIRM) (Zolesi et al., 1993, 1996; Perna et al., 2017a) with the Lockwood algorithm. The most important ionospheric characteristics from the radio propagative point of view, i.e. *fo*F2 and *M*(3000)F2, are output by the SIRM model like monthly median values calculated on the base of the predicted 12-months smoothed sunspots number (R_{12}). Such values are then used in combination with the Lockwood algorithm to calculate the *MUF* values from which *MUF* and *skip distance* climatological maps are generated.

As for the maps provided in the DIAS system, also *MUF* and *skip distance* nowcasting maps are produced applying the SIRMUP&LKW procedure (Pietrella et al., 2009) which uses the SIRMUP model in conjunction with the Lockwood algorithm. This procedure is more complex than the one applied to output climatological maps, because SIRMUP requires the assimilation of ionosonde measurements; the latter, in our case, are recorded every 15 min at the INGV ionospheric observatories of Rome (41.9°N; 12.5°E) and Gibilmanna (37.8°N; 14.0°E) and automatically processed by the Autoscala algorithm. The data assimilation, and their use for the calculation of an effective sunspots number (Houminer et al., 1993), leads to "replace" the monthly median values provided by the SIRM with most accurate *fo*F2 and *M*(3000)F2 nowcasting representations; *fo*F2 and *M*(3000)F2 nowcasting values are then exploited in combination with the Lockwood algorithm to calculate *MUF* values and consequently *MUF* and *skip distance* nowcasting maps.

It is worth highlighting that these new maps (which will be shown in Sections 4 and 5) constitute an advance with respect to the DIAS maps, because they can provide a much more detailed information about the *MUF and skip distance* over Italy than the one provided in the framework of the DIAS project (Belehaki et al., 2005). This happens because DIAS *MUF and skip distance* maps cannot represent in detail the radio propagation conditions over relatively small regions like for example the Italian one.

This paper focuses on the possibility to mitigate space weather effects over Italy providing a quasi real-time specification of the ionosphere through ionosonde measurements. This is realized giving a picture as much reliable as possible of the real radio propagation conditions, which means to supply a real-time support to HF communications, that is extremely important especially for disturbed conditions.

A brief recall on the *skip distance* and *MUF* is given in Sections 2 and 3 respectively. The description of the method to generate *MUF* and *skip distance* climatological maps is provided in Section 4. How the *MUF* and *skip distance* nowcasting maps are generated is the subject of Section 5. The results are discussed in Section 6, while the conclusions and possible future developments form Section 7. Finally, given that Lockwood's algorithm plays an important role in the *MUF* calculation, we decided to specify it in the Appendix A.1, so that the reader could immediately have an idea of its "complexity". Details describing the SIRM&LKW and SIRMUP&LKW procedures are also provided for the benefit of users in the Appendix A.2.

2. A brief reference to the skip distance

The *skip distance* is the minimum distance, over the Earth's surface, between the point where a radio signal of a specified frequency is transmitted and the point where it is received after having been reflected by the ionosphere through a single-hop (see Fig. 1). When neglecting the ground wave coverage, this distance identifies the *silent zone* or *dead zone*, that is, the region where a radio signal cannot be received.

In case of oblique radio propagation, the reflection condition is fulfilled when the transmitted frequency f_T is equal to:

$$f_T = f_P \cdot \sec\phi, \tag{1}$$

where f_P is the plasma frequency measured at the reflection height by means of a vertical ionospheric radio sounding carried out in the middle point of the radio link, and ϕ is the angle of incidence of the electromagnetic wave at the base of the ionosphere; $f_P \cong 9(N)^{1/2}$, where N is the electron density depending on the geographic latitude and longitude, solar declination, local time, and solar activity. Indicating with f_C the critical frequency of the reflecting layer, i.e., the maximum frequency that can be reflected by the layer, from Eq. (1) we get the critical angle ϕ_C (see the red ray in Fig. 1) i.e.:

$$\phi_C = \arccos\frac{f_C}{f_T}. \tag{2}$$

Referring to Fig. 1, the largest angle satisfying the reflection condition is the angle ϕ_T corresponding to the radio signal transmitted almost tangentially to the land surface (see the blue ray in Fig. 1) thus reaching the farthest point (P_D) from the transmitter (T) (*limit distance*). As the angle ϕ decreases, the reflection condition is fulfilled at larger heights and the radio signal reaches distances more and more smaller than the *limit distance* (i.e., points P_3, P_2, and P_1 in Fig. 1), up to a minimum distance that is the *skip distance* (point P_S in Fig. 1). At the *skip distance* the radio signal reflects itself under the angle of incidence ϕ_C. For all radio signals travelling under angles of incidence smaller than ϕ_C (green rays in Fig. 1) there is no way to satisfy Eq. (1), as consequence they "hole" the ionosphere and lose themselves into space. Therefore, the distances for which the radio link at a definite frequency is guaranteed range between the *skip distance* and the *limit distance*.

3. A brief reference to the MUF

In general terms, the secant law (1) establishes that the ionospheric reflection at a height h of an electromagnetic wave transmitted with frequency f_T, takes place when the frequency of the wave is equal to the plasma frequency f_P (which would have been measured at the height h with a vertical radio sounding performed with an ionosonde placed in the middle point of the radio link) times the secant of the angle of incidence ϕ of the electromagnetic wave at the base of the ionosphere (Mc Namara, 1991). Taking into account also the effect of the Earth's curvature (important for *ground ranges* greater than 500 km), the value of $\sec\phi$ can be expressed as:

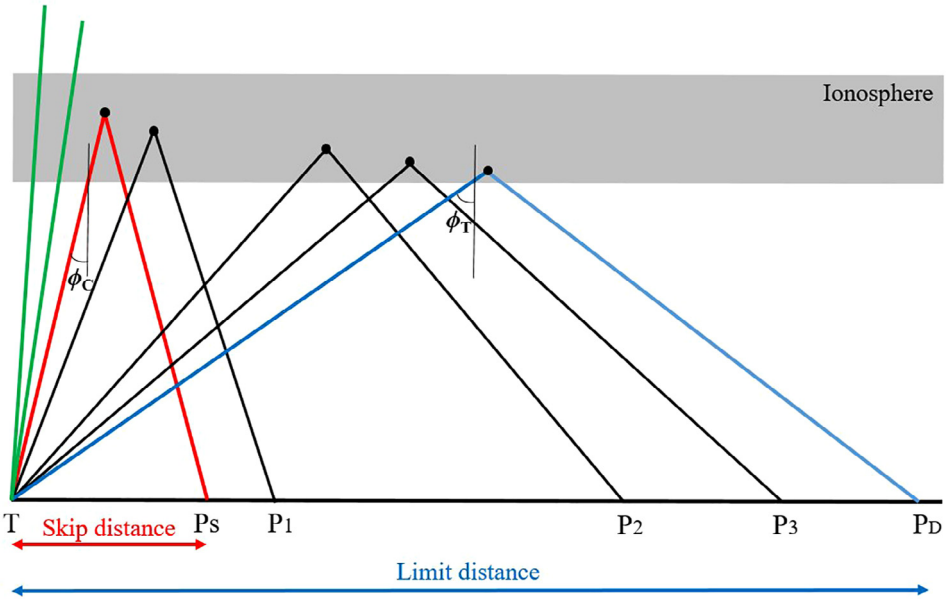

Fig. 1. Sketch showing the reflection conditions for different incidence angles in case of oblique radio propagation at a fixed frequency.

$$\sec\phi = \sqrt{1 + \left[\frac{\sin\frac{D}{2R_T}}{1 + \frac{h}{R_T} - \cos\frac{D}{2R_T}}\right]^2}, \tag{3}$$

being D the *ground range* between the transmitter and the receiver, h the height of the ionospheric reflection point and R_T the Earth's radius (Davies, 1990); $\sec\phi$ is therefore a factor depending essentially on the geometry of the circuit under consideration.

In principle, the *MUF* for an F2 layer single hop and a *ground range* D is that frequency for which the product given by Eq. (1) is maximum. According to this, and considering the ordinary mode of propagation, the *MUF* is usually calculated with a good approximation by the formula

$$MUF_o(D)\mathrm{F2} = fo\mathrm{F2} \cdot \sec\phi; \tag{4}$$

this formula (the subscript "o" means that we are referring to the ordinary mode of propagation) is practically equal to Eq. (1), for which the plasma frequency f_P is replaced with its maximum value, i.e. foF2. Since f_P depends on the geographic latitude and longitude, solar declination, local time, and solar activity, it is clear that for a given radio link the range of usable frequencies, and therefore of the *MUF*, will vary with the location of the transmitting point, season, time of the day, and solar cycle. At this point, it should be noted that there exists the possibility that the radio link is established also through the extraordinary mode of propagation, for which the critical frequency is

$$fx\mathrm{F2} \approx fo\mathrm{F2} + \frac{f_H}{2}, \tag{5}$$

where f_H is the electron gyrofrequency. Consequently, it is also possible to establish successful radio links with frequencies greater than the one given by Eq. (4). Therefore, indicating with $MUF(D)$F2 the maximum usable frequency independently of the propagation mode, this is equal to

$$MUF(\mathrm{D})\mathrm{F2} = fo\mathrm{F2} \cdot sec\phi + \frac{f_H}{2} \cdot \sec\phi. \tag{6}$$

Nevertheless, instead of Eq. (6) we preferred to apply the Lockwood algorithm in which, as described in the Appendix A.1, the form of $\sec\phi$ assumes a rather complex structure in order to achieve a better accuracy. Hereafter $MUF_{LKW}(D)$F2 will indicate the *MUF* calculated with the Lockwood algorithm.

4. MUF and skip distance climatological maps

The INGV Upper Atmosphere Physics unit provides hourly climatological maps of $MUF_o(D)$F2 and *skip distance* with two months in advance, over an area extending in latitude from 34°N to 60°N and in longitude from 5°W to 40°E. This kind of prediction maps are included in the file "*Prediction Tables for the Ionospheric Radiopropagation*" which is uploaded every two months as a *pdf* file downloadable at the address *http://previsioniionosferiche.rm.ingv.it*. Generally, militaries, aviation, the Civil Protection Department, and radio amateurs are the interested users. An example of maps currently delivered is given in Fig. 2.

This kind of maps are generated starting from the monthly median values of $fo\mathrm{F2_S}$ and $M(3000)\mathrm{F2_S}$ calculated by the SIRM model using as input for the solar activity the predicted R_{12} (downloadable at *http://www.sws.bom.gov.au/Solar/1/6*). $fo\mathrm{F2_S}$ and $M(3000)\mathrm{F2_S}$ data are then exploited according to the procedure described in the Appendix A.2 to determine the values of $fo\mathrm{F2_M}$ and

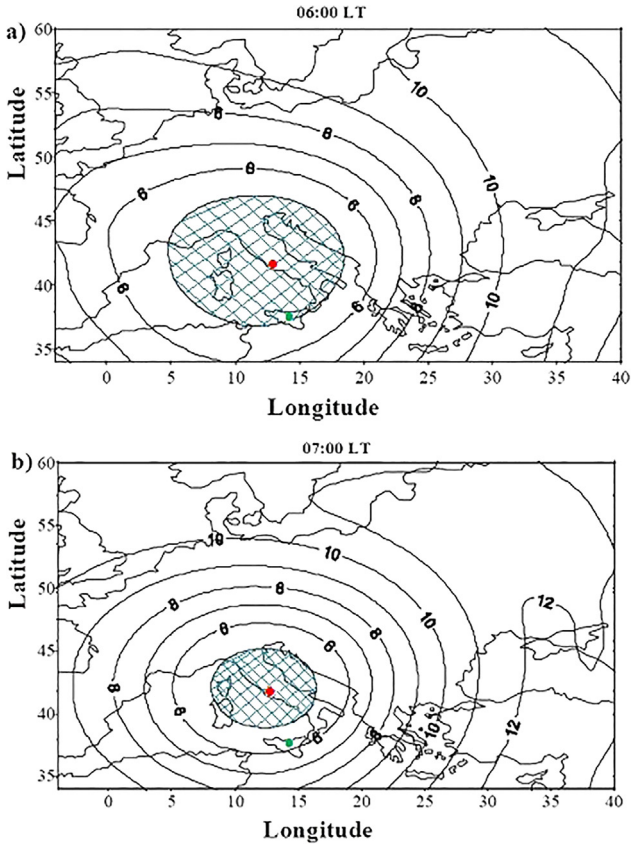

Fig. 2. Isolines of $MUF_o(D)$F2 and corresponding *skip distances* for June 2009: (a) at 06:00 local time the asymmetric distribution is due to the Sun coming from east; (b) at 07:00 local time the asymmetry is almost completely disappeared. The red and green dots mark the position of Rome and Gibilmanna respectively. The blue shadowed areas mark the *silent zone* for 5 MHz, i.e., that zone that cannot be reached by radio signals transmitted from Rome with a frequency of 5 MHz. (For interpretation of the references to colour in this figure legend, the reader is referred to the web version of this article.)

$M(3000)F2_M$ representing the critical frequency and the propagation factor in the middle point of a given link. Finally, $MUF_o(D)$F2 values are calculated by using a very simple algorithm developed at INGV in the early '80s to be applied over relatively small distances; specifically,

$$MUF_o(D)F2 = foF2_M \sec\phi, \tag{7.1}$$

where

$$\sec\phi = \frac{D_K}{\cos\left[\arctan\left(\frac{SNF}{DEN}\right)\right]}, \tag{7.2}$$

with

$$D_K = 0.000047D + 0.973 \text{ if } D < 1000 \text{ and } D_K = 1.01 \text{ if } D \geqslant 1000, \tag{7.3}$$

$$SNF = \sin\left(\frac{D}{12740}\right), \tag{7.4}$$

and

$$DEN = \left[\frac{0.2333086}{\tan\left(\arccos\left(\frac{1.114}{M(3000)F2_M}\right)\right)}\right] + 0.9724027 - \cos\left(\frac{D}{12740}\right). \tag{7.5}$$

Observing the maps of Fig. 2, it is evident that a satisfactory description of both the $MUF_o(D)$F2 and the *skip distance* over Italy is missing because of the low number of isolines centred around Rome. Another fact is that only Rome is considered as transmitting point. This is why we have developed a new software tool aiming at overcoming these constraints, generating climatological maps in a more restricted area extending in latitude from 34°N to 48°N and in longitude from 5°E to 20°E, including the whole Italian territory.

To this purpose the SIRM&LKW procedure explained in the Appendix A.2 was implemented to replace the algorithm described by Eqs. (7). We have made this choice because the scientific community, specifically, the International Telecommunication Union (ITU), recognized this algorithm particularly indicated to achieve a greater accuracy in the *MUF* calculation (CCIR, 1991).

Figs. 3–6 show four examples of $MUF_{LKW}(D)$F2 and *skip distance* climatological maps obtained applying such procedure.

5. MUF and skip distance nowcasting maps

The SIRMUP model is nothing more than the SIRM model with the only difference that SIRMUP uses as input an effective 12-months running mean of the sunspots number, i.e. R_{12eff}, in place of R_{12}. Since R_{12eff} is based on real-time ionosonde observations, its use allows to "update" the SIRM model so as to "nowcast" the ionospheric characteristics *fo*F2 and *M*(3000)F2 and, subsequently, $MUF_{LKW}(D)$F2 and *skip distance* maps. The technique for determining an effective solar activity index was conceived and described in detail by Houminer et al. (1993). Generally speaking, the value of R_{12eff} which is used to update the SIRM model is the one making minimum the mean square error

$$\Delta = \frac{1}{N}\sum_{i=1}^{N}(C_{obs,i} - C_{mod,i})^2 \tag{8}$$

between the observed $C_{obs,i}$ and modelled $C_{mod,i}$ ionospheric characteristic at the reference station i, where N is the number of reference stations.

It is worth specifying that $C_{mod,i}$ values are calculated for different values of R_{12eff} ranging from an initial value R_{12eff_ini} to a final value R_{12eff_fin}, with a definite step s. As a consequence, from Eq. (8) a set of values of $\Delta = \Delta(R_{12eff})$ is calculated and, as already mentioned above, the value of R_{12eff} in correspondence of which $\Delta = \Delta_{min}$ is identified. It is worth highlighting that the value of R_{12eff} so found derives from the real-time ionosonde observations

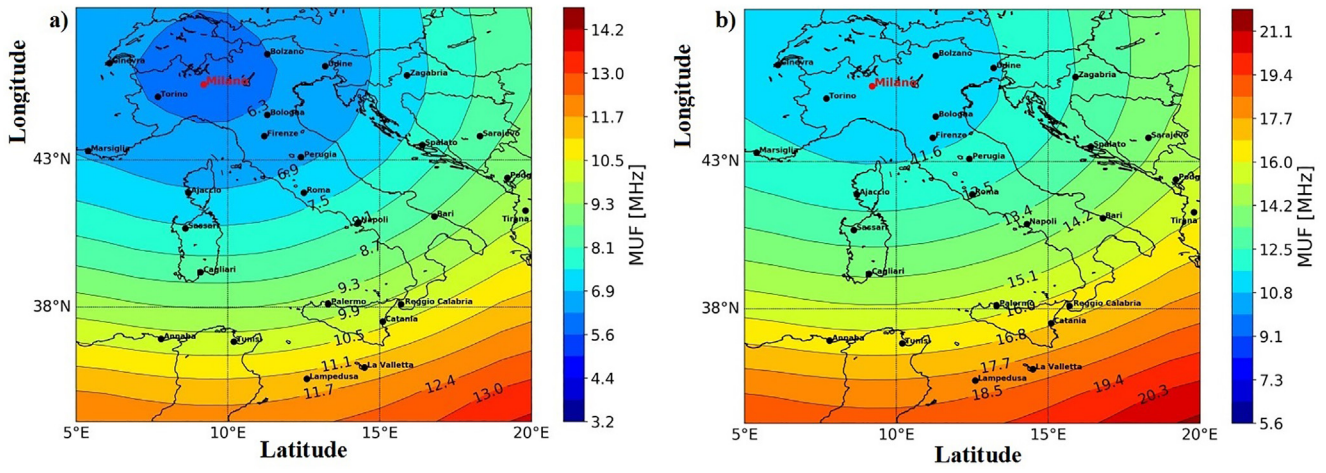

Fig. 3. $MUF_{\mathrm{LKW}}(D)$F2 and *skip distance* climatological maps centred on Milan for September at 14:00 universal time (UT) for (a) low solar activity (LSA, $R_{12} = 10$) and (b) high solar activity (HSA, $R_{12} = 150$).

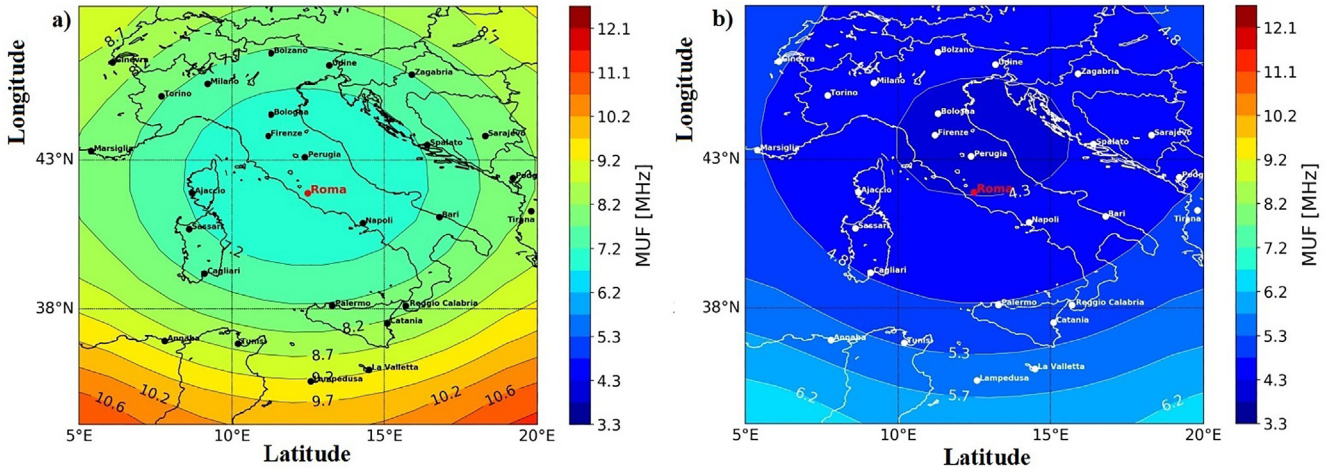

Fig. 4. $MUF_{\mathrm{LKW}}(D)$F2 and *skip distance* climatological maps centred on Rome for April at LSA ($R_{12} = 10$) for (a) daytime at 10:00 UT and (b) nighttime at 23:00 UT.

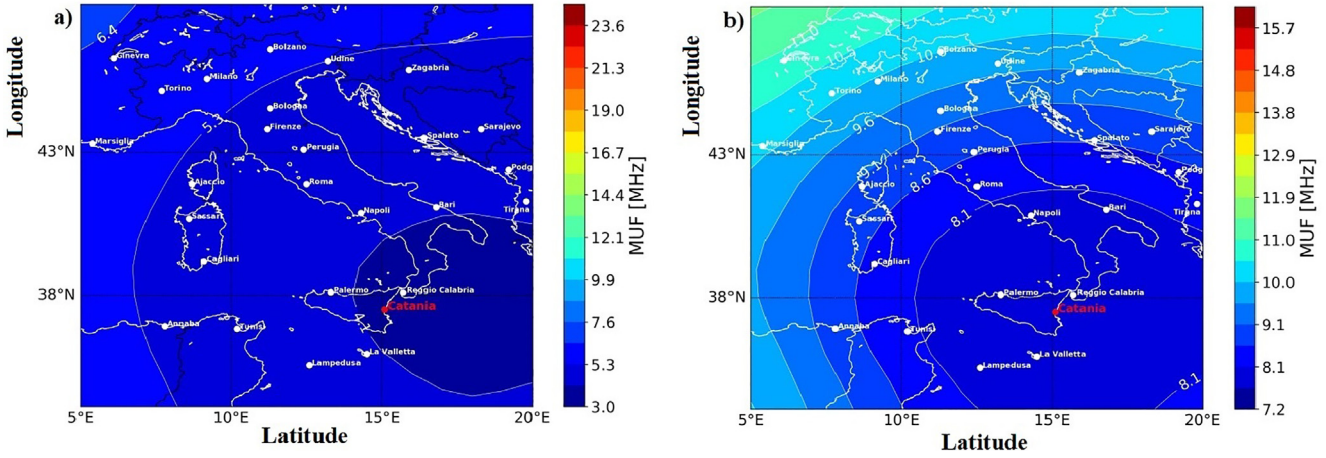

Fig. 5. $MUF_{\mathrm{LKW}}(D)$F2 and *skip distance* climatological maps centred on Catania for nighttime at 02:00 UT, for HSA ($R_{12} = 150$) in (a) winter (January) and (b) summer (July).

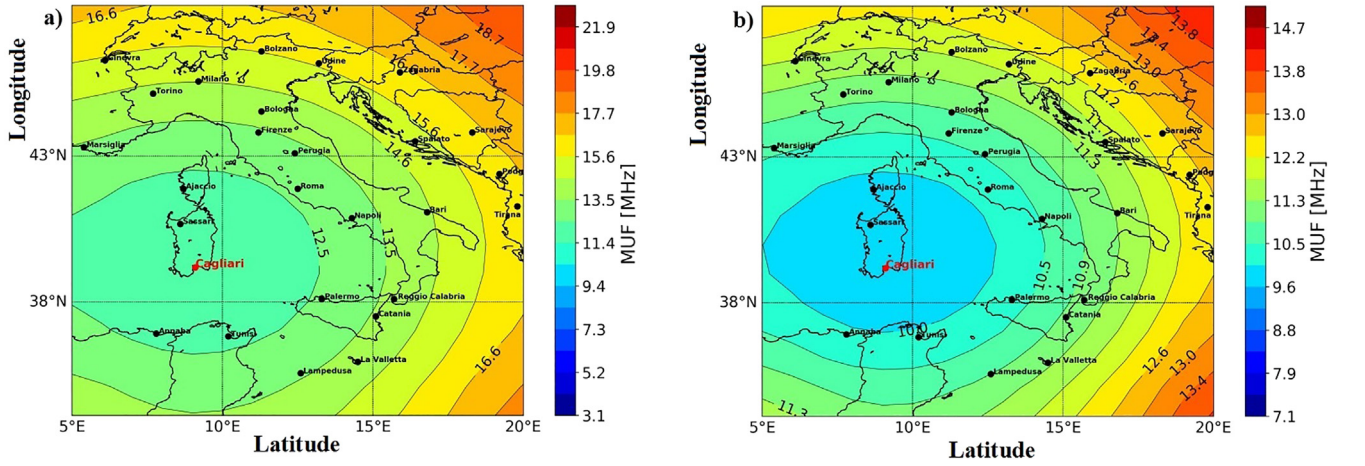

Fig. 6. $MUF_{LKW}(D)$F2 and *skip distance* climatological maps centred on Cagliari for daytime at 12:00 UT, for HSA ($R_{12} = 150$) in (a) winter (January) and (b) summer (July).

that come into play in Eq. (8), which means that the R_{12eff} minimizing Δ is the more appropriate to be used in order to get a picture of the radio propagation conditions as much close as possible to the real one.

In this specific case $N = 2$, because the ionosonde observations used in this study are those recorded and automatically processed by Autoscala at the two INGV ionospheric observatories of Rome, in the central Italy, and Gibilmanna, in the Southern Italy. $C_{obs,i}$ stands for both *fo*F2 and *M*(3000)F2; these two characteristics are simultaneously autoscaled every 15 min in the considered reference station, which means that the procedure above explained provides two different R_{12eff}: one for *fo*F2, i.e. $R_{12eff\ (foF2)}$, and one for *M*(3000)F2, i.e. $R_{12eff\ (M(3000)F2)}$. $C_{mod,i}$ are the values of *fo*F2 and *M*(3000)F2 calculated at Rome and Gibilmanna by the SIRM model assuming $R_{12eff\_ini} = -95$, $R_{12eff\_fin} = 200$, and $s = 5$.

The values of $R_{12eff\ (foF2)}$ and $R_{12eff\ (M(3000)F2)}$ determined every 15 min of a given hour, that is at 00:15, 00:30, 00:45, 01:00, 01:15,. . ..., 23:30, 23:45 UT, are used as input by the SIRM model to calculate respectively the *fo*F2 and *M*(3000)F2 nowcasting representations over each grid point. As shown in the Appendix A.2 such values constitute the starting point to generate $MUF_{LKW}(D)$F2 and *skip distance* nowcasting maps, which will have the same time resolution of ionosonde data, i.e. 15 min.

The need for producing nowcasting maps every 15 min arises from the fact that, in response to important space weather events, the ionospheric variability at time scales shorter than one hour is significant and cannot be neglected. This feature will enable HF users to face periods of adverse radio propagation conditions, in terms of frequency usage and management planning. Figs. 7–12 show examples of nowcasting maps generated after applying the SIRMUP&LKW procedure described in the Appendix A.2; Table 1 shows corresponding values of *fo*F2 and *M*(3000)F2 autoscaled by Autoscala at the two reference stations of Rome and Gibimanna and then used to determine $R_{12eff\ (foF2)}$ and $R_{12eff\ (M(3000)F2)}$ through Eq. (8).

Once again we want to point out that the generation of $MUF_{LKW}(D)$F2 and *skip distance* nowcasting maps over Italy, with a time resolution of 15 min, represents the main result of this study. The need to generate nowcasting maps stems from the fact that currently only $MUF_o(D)$F2 and *skip distance* climatological maps, with a time resolution of one hour, are available (see *http://previsioniionosferiche.rm.ingv.it*), that are unreliable when important space weather events occur. To be aware of this matter we can refer to Fig. 13 showing the ionospheric effects observed in Italy in response to one of the strongest magnetic storms ever recorded in this century, caused by a series of intense solar events occurred in March 1989 (e.g. Bianchi et al., 1992). The drastic changes occurred in the F region are rather evident in terms of the hourly *fo*F2 behaviour; in particular, both in Rome and Gibilmanna, *fo*F2 values observed on 13 March 1989 are by far smaller than corresponding monthly median values representative of a quiet ionosphere. Fig. 13 shows also the *fo*F2 hourly deviations from the climatological behaviour calculated by the SIRM model applied over Rome during the severe magnetic storm occurred in the early days of October 2013; once again, *fo*F2 observed values are much smaller than the ones characterizing quiet ionospheric conditions.

Therefore, during a negative ionospheric phase (i.e. real values lower than climatological ones) as the one shown in Fig. 13, the *MUF* can be by far lower than that normally working in case of a quiet ionosphere; in this case, a frequency transmitted around the climatological value would pass through the ionosphere, being never reflected. This means that $MUF_{LKW}(D)$F2 and *skip distance* climatological maps like those represented in Figs. 3–6 would be misleading for space weather purposes. This is rather evident comparing the climatological maps of Fig. 14, for March 1989 at 12:00 UT and October 2013 at 09:00 UT, with

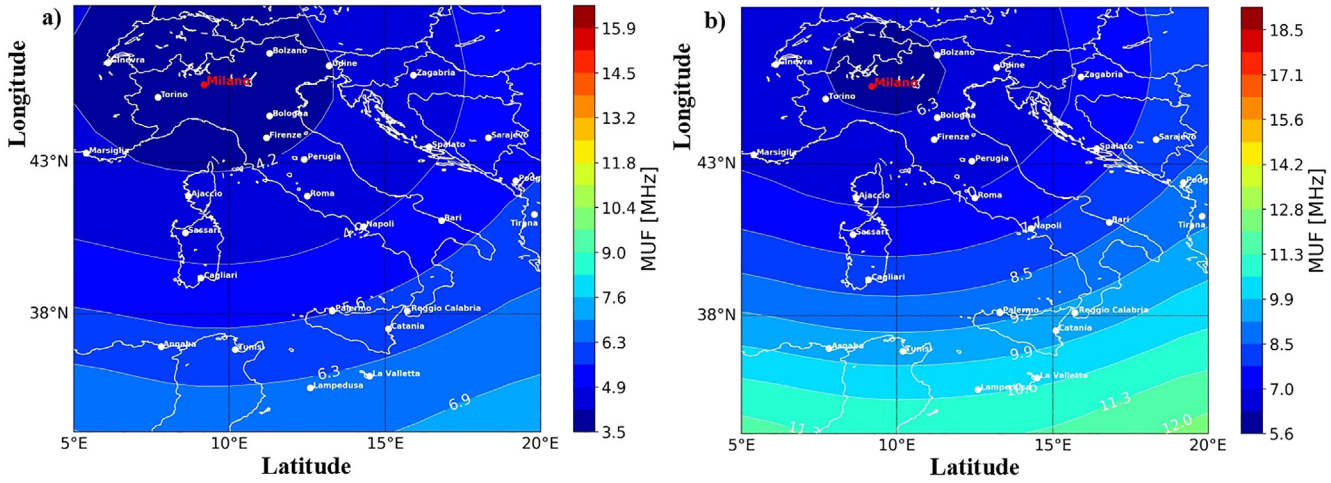

Fig. 7. $MUF_{LKW}(D)$F2 and *skip distance* nowcasting maps centred on Milan on (a) 20 July 2018 at 01:15 UT, for $R_{12eff\ (foF2)} = +5$ and $R_{12eff\ (M(3000)F2)} = -95$, and on (b) 22 July 2014 at 01:15 UT, for $R_{12eff\ (foF2)} = +95$ and $R_{12eff\ (M(3000)F2)} = -50$.

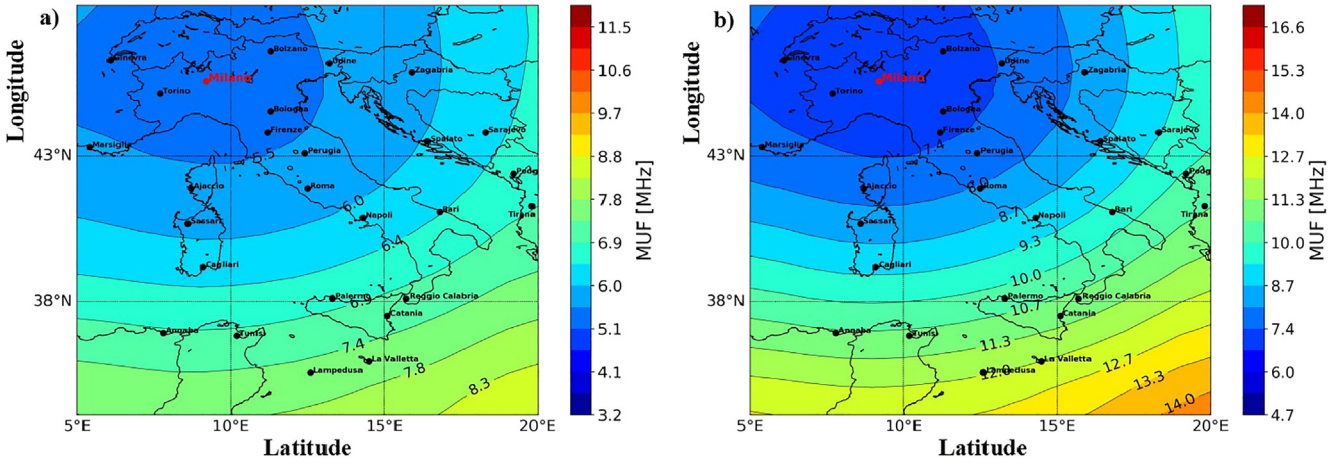

Fig. 8. $MUF_{LKW}(D)$F2 and *skip distance* nowcasting maps centred on Milan on (a) 20 July 2018 at 12:30 UT, for $R_{12eff\ (foF2)} = -10$ and $R_{12eff\ (M(3000)F2)} = +200$, and on (b) 22 July 2014 at 12:30 UT, for $R_{12eff\ (foF2)} = +55$ and $R_{12eff\ (M(3000)F2)} = -30$.

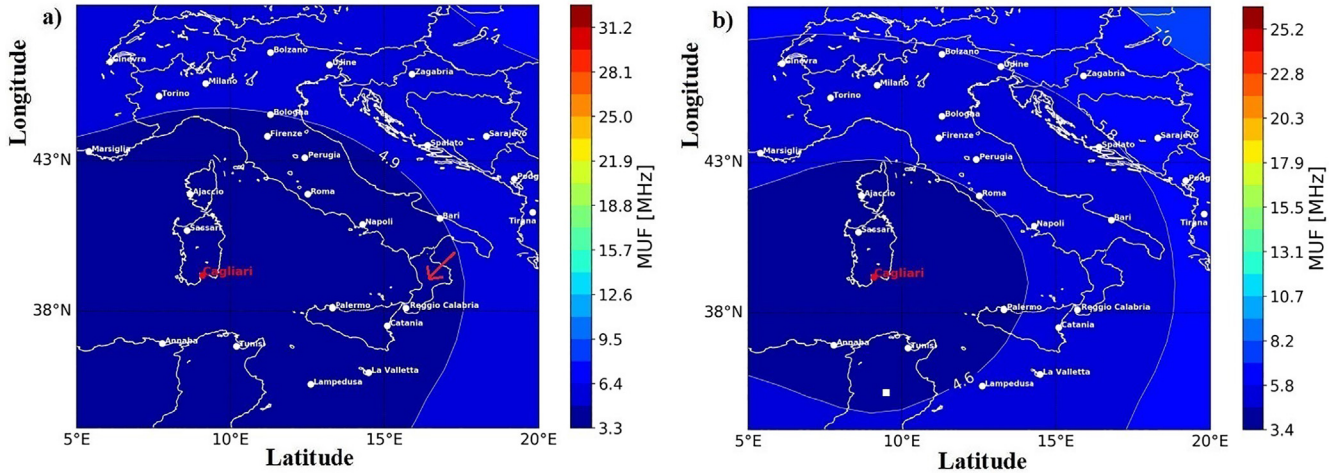

Fig. 9. $MUF_{LKW}(D)$F2 and *skip distance* nowcasting maps centred on Cagliari on (a) 10 December 2007 at 00:30 UT, for $R_{12eff\ (foF2)} = +140$ and $R_{12eff\ (M(3000)F2)} = -95$, and on (b) 10 December 2013 at 00:30 UT, for $R_{12eff\ (foF2)} = +110$ and $R_{12eff\ (M(3000)F2)} = -50$.

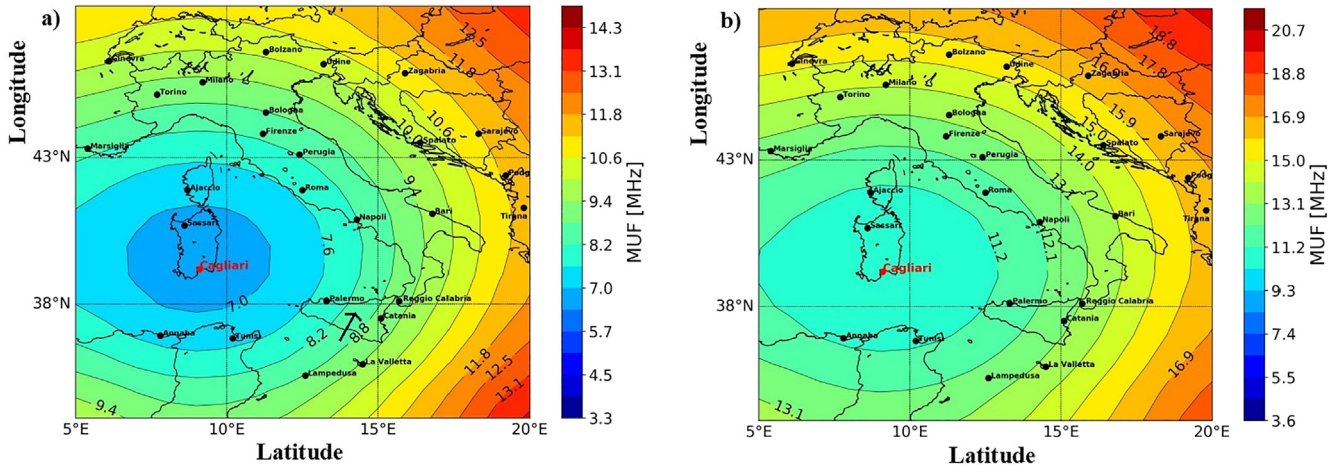

Fig. 10. $MUF_{\mathrm{LKW}}(D)$F2 and *skip distance* nowcasting maps centred on Cagliari on a) 10 December 2007 at 11:30 UT, for $R_{12\mathrm{eff}\ (foF2)} = +10$ and $R_{12\mathrm{eff}\ (M(3000)F2)} = -35$, and on 10 December 2013 at 11:30 UT, for $R_{12\mathrm{eff}\ (foF2)} = +100$ and $R_{12\mathrm{eff}\ (M(3000)F2)} = +70$.

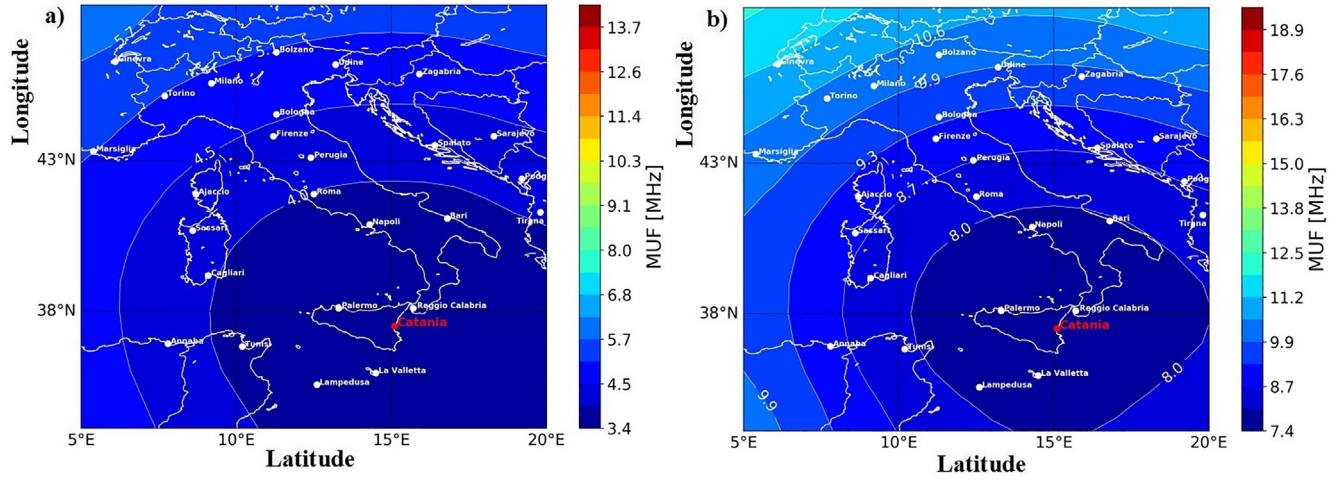

Fig. 11. $MUF_{\mathrm{LKW}}(D)$F2 and *skip distance* nowcasting maps centred on Catania on (a) 9 May 2008 at 02:45 UT, for $R_{12\mathrm{eff}\ (foF2)} = -5$ and $R_{12\mathrm{eff}\ (M(3000)F2)} = -30$ and on (b) 15 May 2013 at 02:45 UT, for $R_{12\mathrm{eff}\ (foF2)} = +135$ and $R_{12\mathrm{eff}\ (M(3000)F2)} = +60$.

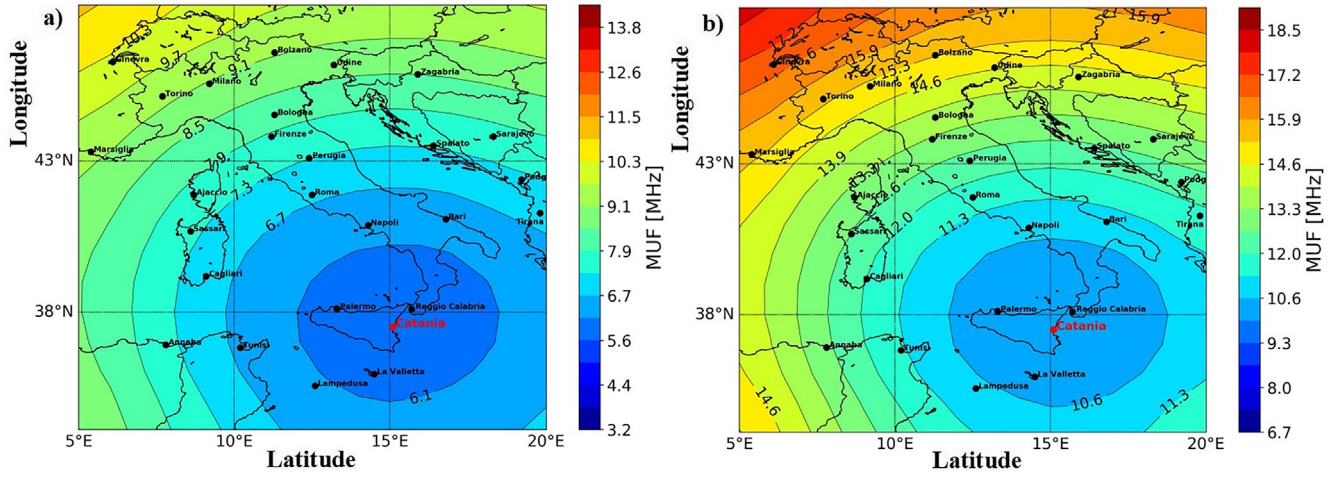

Fig. 12. $MUF_{\mathrm{LKW}}(D)$F2 and *skip distance* nowcasting maps centred on Catania on (a) 9 May 2008 at 13:45 UT, for $R_{12\mathrm{eff}\ (foF2)} = -15$ and $R_{12\mathrm{eff}\ (M(3000)F2)} = -65$ and on (b) 15 May 2013 at 13:45 UT, for $R_{12\mathrm{eff}\ (foF2)} = +110$ and $R_{12\mathrm{eff}\ (M(3000)F2)} = 0$.

Table 1
Autoscaled *fo*F2 and *M*(3000)F2 data and corresponding effective indices $R_{12\text{eff }(foF2)}$ and $R_{12\text{eff }(M(3000)F2)}$ used to generate nowcasting maps shown in Figs. 7–12.

Epoch	Rome *fo*F2(MHz)/*M*(3000)F2	Gibilmanna *fo*F2(MHz)/*M*(3000)F2	$R_{12\text{eff }(foF2)}$	$R_{12\text{eff }(M(3000)F2)}$
20 July 2018-01:15 UT	3.40/3.21	3.20/3.19	+5	−95
22 July 2014-01:15 UT	5.80/3.10	5.90/3.07	+95	−50
20 July 2018-12:30 UT	5.10/2.43	4.90/2.49	−10	+200
22 July 2014-12:30 UT	6.30/3.11	6.90/3.16	+55	−30
10 December 2007-00:30 UT	3.30/3.24	3.20/3.25	+140	−95
10 December 2013-00:30 UT	3.70/3.05	3.60/3.28	+110	−50
10 December 2007-11:30 UT	5.60/3.80	660/3.89	+10	−35
10 December 2013-11:30 UT	9.00/3.43	10.10/3.36	+100	+70
9 May 2008-02:45 UT	2.90/3.24	2.90/3.14	−5	−30
15 May 2013-02:45 UT	6.80/2.84	6.80/2.93	+135	+60
9 May 2008-13:45 UT	5.00/3.22	5.50/3.29	−15	−65
15 May 2013-13:45 UT	8.90/3.11	9.50/3.09	+110	0

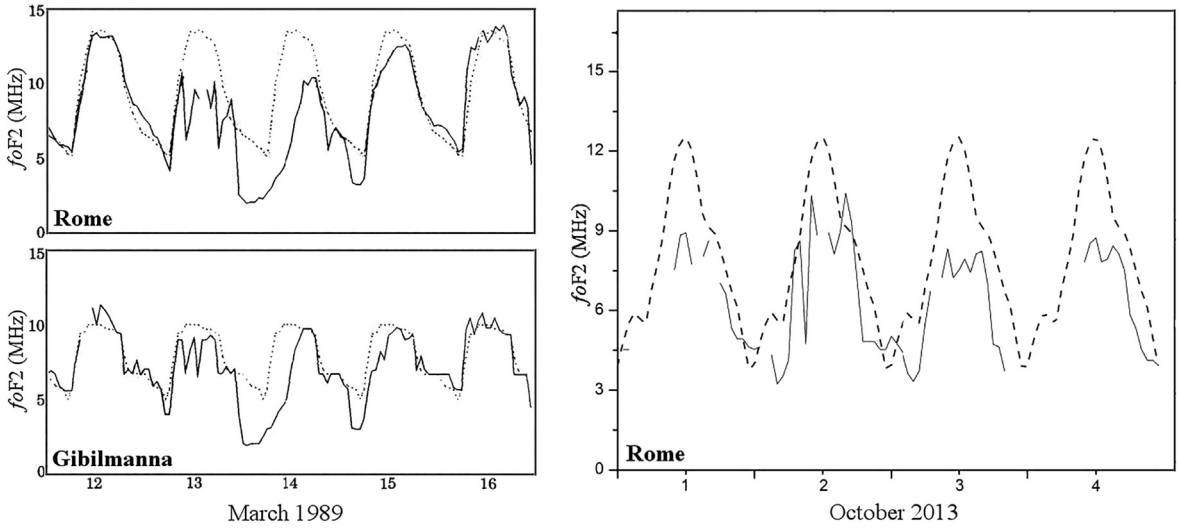

Fig. 13. (Left) Measured (full line) and monthly median (dotted line) *fo*F2 values at (upper panel) Rome and (bottom panel) Gibilmanna from 12 to 16 March 1989. (Rearranged from Bianchi et al. (1992)). (Right) Measured (full line) and SIRM modelled (dashed line) *fo*F2 values at Rome from 1 to 4 October 2013.

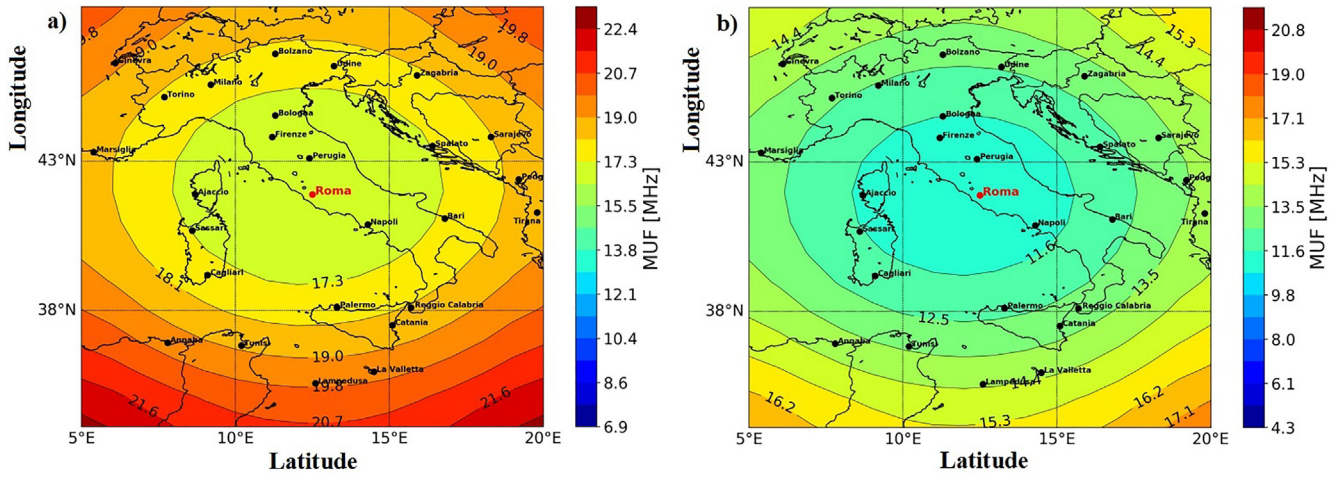

Fig. 14. $MUF_{LKW}(D)$F2 and *skip distance* climatological maps centred on Rome on (a) March 1989 at 12:00 UT ($R_{12} = 198$) and on (b) October 2013 at 09:00 UT ($R_{12} = 107$).

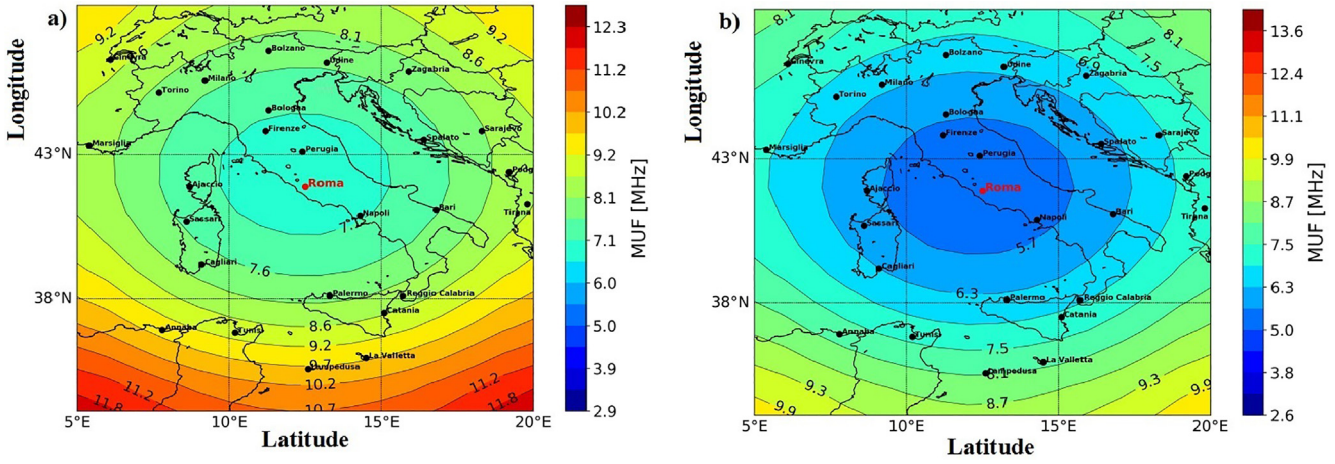

Fig. 15. $MUF_{\mathrm{LKW}}(D)$F2 and *skip distance* nowcasting maps centred on Rome on (a) 13 March 1989 at 12:00 UT ($R_{12\mathrm{eff}\ (foF2)} = 5$ and $R_{12\mathrm{eff}\ (M(3000)F2)} = -10$) and on (b) 2 October 2013 at 09:00 UT ($R_{12\mathrm{eff}\ (foF2)} = -25$ and $R_{12\mathrm{eff}\ (M(3000)F2)} = -90$).

the corresponding nowcasting maps of Fig. 15 obtained on 13 March 1989 at 12:00 UT and on 2 October 2013 at 09:00 UT, representing the two epochs related to very disturbed ionospheric conditions over Italy, as shown in Fig. 13.

The nowcasting map shown in Fig. 15a was generated exploiting the measurements of *fo*F2 = 6.6 MHz and *M*(3000)F2 = 3.44 taken at Gibilmanna (data from Rome was unavailable) on 13 March 1989 at 12:00 UT. For sake of clarity, to obtain this nowcasting map manually validated data have been used because at that time the software capable to autoscale ionograms at Rome and Gibilmanna was not yet available. Likewise the nowcasting map of Fig. 15b was generated exploiting the measurements of *fo*F2 = 4.7 MHz and *M*(3000)F2 = 3.79 autoscaled at Rome (data from Gibilmanna was unavailable) on 2 October 2013 at 09:00 UT.

6. Discussion

$MUF_{\mathrm{o}}(D)$F2 and *skip distance* climatological maps provided by INGV since 1988 refer to a very large area and, for this reason, cannot provide a detailed overview of radio propagation conditions over the Italian region. The two procedures SIRM&LKW and SIRMUP&LKW, applied over a sector extending in latitude from 34°N to 48°N and in longitude from 5°E to 20°E, generate climatological and nowcasting maps characterized by a new graphic design, an increased number of isolines, and four transmitting points, thus permitting to get a more detailed info about the radio propagation conditions in terms of $MUF_{\mathrm{LKW}}(D)$F2 and *skip distance* over the Italian territory.

Fig. 3 shows two climatological maps obtained for September at 14:00 UT, simulating a transmitter placed in Milan; as expected, the LSA map shows $MUF_{\mathrm{LKW}}(D)$F2 values smaller than those shown by the HSA map. Specifically, due to the less energetic electromagnetic and corpuscular emission from the Sun during LSA, the level of ionization in the ionosphere lowers and $MUF_{\mathrm{LKW}}(D)$F2 values vary from 6.1 MHz to 14.1 MHz; on the contrary, the more energetic solar electromagnetic and corpuscular emission occurring in case of HSA increases the level of ionization in the ionosphere, and $MUF_{\mathrm{LKW}}(D)$F2 values vary from 11.0 MHz to 21.9 MHz. These rather significant differences show how the solar activity plays an important role in determining $MUF_{\mathrm{LKW}}(D)$F2 values.

Fig. 4 shows two climatological maps obtained for April, for LSA, simulating a transmitter placed in Rome, highlighting that also the hour of the day plays an important role in determining $MUF_{\mathrm{LKW}}(D)$F2 values: during daytime, at 10:00 UT, due to the electromagnetic solar radiation, $MUF_{\mathrm{LKW}}(D)$F2 values vary from 6.7 MHz to 11.7 MHz, while during nighttime, at 23:00 UT, in absence of photoionization, $MUF_{\mathrm{LKW}}(D)$F2 values are smaller varying from 4.1 MHz to 6.8 MHz.

Fig. 5 shows two climatological maps obtained during nighttme at 02:00 UT for HSA simulating a transmitter placed in Catania, highlighting how the mapping is affected by the season; in summer $MUF_{\mathrm{LKW}}(D)$F2 values are greater than those obtained in winter: due to the greater value of the solar declination (21.18°) occurring in July, $MUF_{\mathrm{LKW}}(D)$F2 values range between 7.6 MHz and 11.8 MHz, while the smaller value of the solar declination (−20.92°) occurring in January determines $MUF_{\mathrm{LKW}}(D)$F2 values varying from 4.0 MHz to 6.8 MHz.

Fig. 6 shows instead two $MUF_{\mathrm{LKW}}(D)$F2 and *skip distance* climatological maps obtained during daytime at 12:00 UT for HSA simulating a transmitter placed in Cagliari. It is noteworthy that, differently from the previous case, in summer $MUF_{\mathrm{LKW}}(D)$F2 values vary from 9.7 MHz to 14.6 MHz and they are smaller than those obtained in winter when $MUF_{\mathrm{LKW}}(D)$F2 values vary from 11.7 MHz to 20.2 MHz. The different behaviour observed between night and day reflects the so called "*winter anomaly*", i.e. *fo*F2 daytime values are greater in winter than in

summer, while the contrary happens after the sunset (Rishbeth and Garriot, 1969; Rishbeth et al., 2000; Ezquer et al., 2014; Perna et al., 2017b). The "*winter anomaly*" is always present in the Northern hemisphere at middle latitudes. It is thought to be due to seasonal changes in the molecolar-atomic ratio of the neutral atmosphere causing a larger loss rate in summer. The increase in summer losses exceeds the increase in production, thus resulting in a total ionization of the F2 layer which is actually lower in summer months (Davies, 1990). These considerations demonstrate that climatological maps shown in Figs. 3–6 are consistent with the physics of the ionosphere, confirming the validity of the SIRM&LKW procedure and, consequently, the reliability of corresponding maps.

To better explain the different ways in which these maps can be interpreted we refer to nowcasting ones shown in Figs. 7–12.

Fig. 7 shows the radio propagation conditions during nighttime for two different epochs, by considering Milan as the transmission point. The nowcasting map of the 20 July 2018 at 01:15 UT ($R_{12} = 7.0$) tells us that Florence is situated inside the *silent zone* for the 4.2 MHz isoline. This means that a frequency of 4.2 MHz transmitted from Milan cannot be used to establish a successful radio link with Florence, because higher than the low levels of ionization occurring at this epoch. Therefore, a frequency lower than 4.2 MHz is needed. Specifically, such frequency is not directly quantifiable because the value of the isoline passing over Florence is unkown. Nevertheless, taking into account a step of 0.7 MHz among the various isolines, we can reasonably estimate that with respect to the 3.9 MHz isoline, Florence is beyond the *silent zone* and therefore such frequency is appropriate to carry out the link Milan- Florence. On the other hand, a frequency of 4.2 MHz can be used to establish a successful radio link with Rome. This is possible because Rome is situated beyond the *silent zone* identified by the 4.2 MHz isoline. The map of the 22 July 2014 at 01:15 UT ($R_{12} = 113$) suggests us that frequencies 6.3 and 7.0 MHz can be used to perform successful radio links with Florence and Rome being these towns situated beyond the *silent zone* identified respectively by the 6.3 and 7.0 MHz isolines. In addition, we observe that Naples falls just over the 4.9 MHz isoline on 20 July 2018 at 01:15 UT and the 7.7 MHz isoline on 22 July 2014 at 01:15 UT, meaning that the radio link Milan-Naples can be established by waves travelling with these two frequencies and affecting the ionosphere just under the critical angle. The larger values of usable frequencies characterizing this latter case have to be ascribed to the corresponding higher level of solar activity.

Fig. 8 shows the radio propagation conditions during daytime for the same epochs of Fig. 7. Obviously, due to higher levels of ionization, the usable frequencies are in this case higher. Taking into account the steps among the various isolines, the map for the epoch 20 July 2018 at 12:30 UT suggests that the radio links Milan-Florence, Milan-Rome, and Milan-Naples can be performed with frequencies of 5.0, 5.75, and 6.0 MHz respectively, because it is realistic to guess the three towns beyond the *silent zone* defined by these frequencies. Analogously, consulting the map for the epoch 22 July 2014 at 12:30 UT, we can deduce that the above mentioned radio links can be safely done with frequencies of 7.0, 7.7, and 8.7 MHz. Again, we note how the level of solar activity plays a very important role in determining the range of usable frequencies.

Fig. 9 shows the radio propagation conditions during nighttime for two different epochs, by considering Cagliari as the transmission point. The nowcasting map of 10 December 2007 at 00:30 UT, referring to very LSA ($R_{12} = 8.0$), tells us that transmitting from Cagliari with a frequency of 4.9 MHz we could not perform any radio link with the Calabria Region (indicated on the map with a red arrow) because it is wholly included in the *silent zone* defined by the 4.9 MHz isoline. The nowcasting map of 10 December 2013 at 00:30 UT, referring to HSA ($R_{12} = 108$), shows that such region is situated halfway between the 4.6 and 5.8 MHz isolines. This suggests that the Calabria Region is more or less centred over the 5.2 MHz isoline and it is therefore reasonable that it is not included in the *silent zone* delimited by the 4.9 MHz isoline. Hence, differently from the previous case, the higher solar activity promotes the use of the frequency 4.9 MHz to establish successful radio links with the Calabria Region.

Fig. 10 shows the radio propagation conditions during daytime for the same epochs of Fig. 9. The 10 December 2007 at 11:30 UT the Sicily (indicated on the map with a black arrow) is wholly included between the 7.6 and 9.4 MHz isolines, while the 10 December 2013 at 11:30 UT it is included in the zone delimited by the 11.2 and 13.1 MHz isolines. This implies that any radio link with the Sicily is assured varying properly the frequencies transmitted from Cagliari in the range 7.6–9.4 MHz in case of LSA and in the range 11.2–13.1 MHz in case of HSA.

From the nowcasting map of 9 May 2008 at 02:45 UT (Fig. 11a), referring to very LSA ($R_{12} = 5$), it is observed that the Corsica is presumably included between the 4.25 and 4.5 MHz isolines, while the nowcasting map of 9 May 2008 at 13:45 UT (Fig. 12a), indicates that the Corsica is included between the 7.3 and 7.9 MHz isolines. This imply that the Corsica is reachable varying appropriately the frequencies transmitted from Catania in the range 4.25–4.50 MHz during nighttime, and in the range 7.3–7.9 MHz during daytime. Looking at the nowcasting maps of 15 May 2013 at 02:45 UT (Fig. 11b), and 15 May 2013 at 13:45 UT (Fig. 12b), referring to mid-high solar activity ($R_{12} = 87$), we can deduce that any radio link with the Corsica can be carried out varying properly the frequencies transmitted from Catania in the range 8.7–9.3 MHz during nighttime and in the range 12.6–13.3 MHz during daytime.

The possibility to generate nowcasting maps over the Italian region by considering the ionosonde stations of Rome and Gibilmanna as data provider is the most important aspect of this study. As we are going to see, the availability of nowcasting maps is appreciated above all in case

of important space weather events as for example those occurred in March 1989 and October 2013.

In case of quiet ionospheric conditions for March 1989 at 12:00 UT, one user can consult the map of Fig. 14a deducing that only frequencies transmitted from Rome in the range ≈16–23 MHz can be used to plan radio links. However, if these frequencies had been used on 13 March 1989 at 12:00, during the development of the aforementioned geomagnetic storm, they would pass through the ionosphere, being never reflected. To know the proper frequencies usable in this circumstance, we have to refer to the nowcasting map of Fig. 15a which tells us that the frequencies to be used for a successful radio link over the area under consideration are those in the range ≈7–13 MHz, therefore by far smaller than the climatological ones. Specifically, under quiet ionospheric conditions, looking at the map of Fig. 14a, *skip distances* for the frequency 17.3 MHz are equal to the distances of the radio links Rome - Sassari and Rome - Spalato, because the 17.3 MHz isoline falls just over Sassari and Spalato. This means that an electromagnetic wave of frequency 17.3 MHz affects the ionosphere just under the critical angle and therefore can be used to establish such radio links. For a very disturbed ionosphere like that occurring on 13 March 1989 at 12:00 UT, 17.3 MHz would be a frequency too high to be reflected via ionosphere. Observing the map of Fig. 15a, we note that the *skip distances* for the frequency 7.6 MHz are greater than the distances Rome - Sassari and Rome - Spalato, because the 7.6 MHz isoline includes both Sassari and Spalato; the two towns are therefore situated inside the *silent zone* for the frequency 7.6 MHz which is consequently unavailing for such radio links. Being Sassari and Spalato positioned beyond the 7.1 MHz isoline they fall outside the *silent zone* related to this frequency. A frequency of 7.1 MHz transmitted from Rome is therefore suitable to establish a radio link with these two towns.

The map of Fig. 14b tells us that, under quiet ionosperic conditions in October 2013 at 09:00 UT, only the frequencies transmitted from Rome in the range ≈11–18 MHz are appropriate to plan radio links. On the other hand, if this same range of frequencies had been used during the disturbed conditions occurred the 2 October 2013 at 09:00, they would pass through the ionosphere, being never reflected. To understand which frequencies should have been used in this circumstance, we have to refer to the nowcasting map of Fig. 15b, that tells us that the proper frequencies are those in the range ≈5–11 MHz, therefore by far smaller than the climatological ones. In particular, under quiet ionospheric conditions, looking at the map of Fig. 14b, *skip distances* for the frequency 12.5 MHz can be practically assumed equal to the distances of the radio links Rome–Milan and Rome–Udine, because the 12.5 MHz isoline falls almost over these two towns. This means that the ionosphere is affected by an electromagnetic wave of frequency 12.5 MHz practically under the critical angle, and therefore the frequency 12.5 MHz is appropriate to perform such radio links. For a very disturbed ionosphere like that occurring on 2 October 2013 at 09:00 UT, the frequency 12.5 MHz is too high to be reflected via ionosphere. The nowcasting map of Fig. 15b shows that Milan and Udine are placed inside the *silent zone* for the frequency 6.9 MHz which is therefore unsuccessful for the radio links Rome–Milan and Rome–Udine. At the same time, Milan and Udine are located beyond the 6.3 MHz isoline and hence outside the *silent zone* related to this frequency; so this frequency can be used to establish successful radio links Rome–Milan and Rome–Udine.

The reduction of *MUF* values from the range 16–23 MHz to 7–13 MHz in March 1989, and from the range 11–18 MHz to 5–11 MHz in October 2013, indicates that switching from quiet to very disturbed ionospheric conditions, the usable frequencies over a given area can drastically change.

7. Conclusions and future developments

The considerations made in Section 6 highlight how nowcasting maps, obtained through autoscaled ground-based measurements, and providing a real picture of the radio propagation conditions, can have a great importance in mitigating the effects of severe and strong magneto-ionospheric storms in terms of frequency usage and management planning. In particular, corresponding operational applications are very important for HF users, such as militaries, aviation and the Civil Protection Department since they are intended to guarantee the radio communications among critical infrastructures also in case of adverse space weather conditions. It is worth mentioning that a product like the one here proposed is being implemented also by other European Countries creating National Space Weather services meaning that, in the long run, National services could be unified to provide a unique European service.

With regard to the future developments, the procedures here described can be adopted to get detailed nowcasting maps also over relatively limited European areas with the transmitting points positioned over places of strategic importance such as for instance military infrastructures and airports. In addition, we are going to develop a dedicated web site where climatological maps will be provided with three months in advance and nowcasting maps will be generated and publicly visible every 15 min.

Acknowledgements

The authors are grateful to Dr Silvia Pau and Dr Bruno Zolesi for the help given about the "*Prediction Tables for the Ionospheric Radiopropagation*".

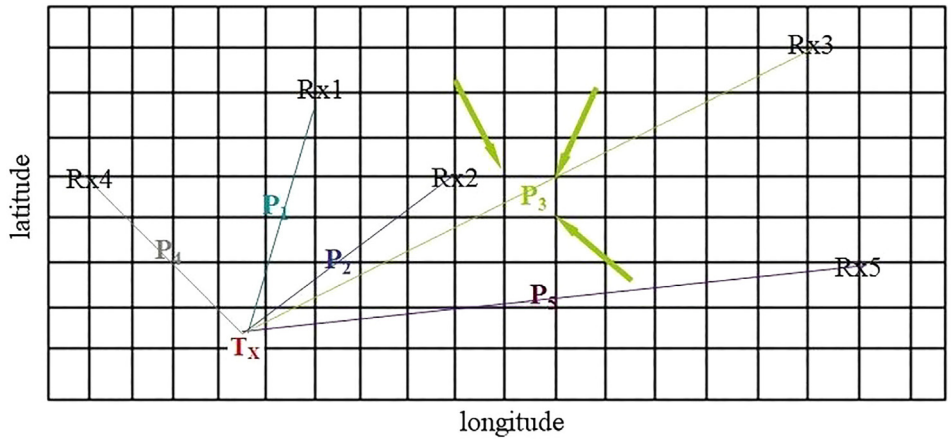

Fig. A2.1. An helpful sketch to understand how the SIRM&LKW and SIRMUP&LKW procedures obtain the final $MUF_{LKW}(D)$F2 values.

Appendix A.1. *The Lockwood algorithm*

In order to achieve a greater accuracy, Eq. (6) is replaced in this study with the following Lockwood algorithm, valid for an F2 layer single hop:

$$MUF_{LKW}(D)F2 = foF2_M\left[1+\left(\frac{C_D}{C_{3000}}\right)(B-1)\right] + \frac{f_H}{2}\left(1-\frac{D}{4000}\right), \quad (A1.1)$$

where

$$C_D = 0.72 - 0.628Z - 0.451Z^2 - 0.03Z^3 + 0.194Z^4 + 0.158Z^5 + 0.037Z^6, \quad (A1.2)$$

With

$$Z = 1 - \frac{2D}{D_{max}}, \quad (A1.3)$$

$$D_{max} = 3940 + \left(9900 + \frac{15375}{x^2} + \frac{106700}{x^5}\right)\left(\frac{1}{B} - 0.258\right), \quad (A1.4)$$

and

$$B = M(3000)F2_M - 0.124 + \left(M(3000)F2_M^2 - 4\right)\left[0.0215 + 0.005\sin\left(\frac{7.854}{x} - 1.9635\right)\right]; \quad (A1.5)$$

D and D_{max} are in kilometres, C_{3000} is the value of C_D for $D = 3000$ km.

The x in (A1.5) is

$$x = \frac{foF2_M}{foE_M} \text{ if } \frac{foF2_M}{foE_M} \geqslant 2 \text{ or } x = 2 \text{ if } \frac{foF2_M}{foE_M} < 2, \quad (A1.6)$$

where $foF2_M$ and foE_M are the ordinary critical frequencies of F2 and E layers respectively, calculated in the middle point of the link.

$M(3000)F2_M$ is the secant of the optimum angle at which to broadcast a signal that is to be received at a distance of 3000 km, calculated in the middle point of the link.

In our case foE_M was calculated through the following long term prediction model

$$foE_M = 3.2[(1 + 0.008R)\cos\chi]^{0.25}, \quad (A1.7)$$

proposed by Dominici (1971); R is the sunspots number and

$$\cos\chi = \sin\varphi\sin\delta + \cos\varphi\cos\delta\cos\omega, \quad (A1.8)$$

where χ is the solar zenith angle, φ is the geographic latitude, δ is the solar declination ranging between $-22°\ 27'$ (at winter solstice) and $+22°\ 27'$ (at summer solstice), and ω is the hourly angle.

Appendix A.2. *SIRM&LKW and SIRMUP&LKW procedures*

The SIRM&LKW and SIRMUP&LKW procedures used to calculate the final $MUF_{LKW}(D)$F2 values, are based on 7 fundamental steps.

Referring to Fig. A2.1:

(1) SIRM and SIRMUP models provide $foF2_S$ and $M(3000)F2_S$ values over each grid point of coordinate φ(latitude) and λ (longitude), at a given hour, month, and solar activity. In the specific case the grid extends in latitude from 34°N to 48°N and in longitude from 5°E to 20°E with a spatial resolution of 1° × 1°.
(2) The distances D_{ji} and the coordinates (φ_{ji}, λ_{ji}) of corresponding middle points P_{ji} are calculated for each link (Tx_j -Rx_i) (j = 1, 2, 3,…, N_{TX} and i = 1, 2, 3,…, N_{RX}, where N_{TX} and N_{RX} are the number of transmitting and receiving points, respectively) starting from the known coordinates of the transmitter (Tx_j) and receiving (Rx_i) points. Specifically, N_{TX}= 4: Tx_1 = Milan (45.5°N; 9.2°E), Tx_2 = Rome (41.9°N; 12.5°E), Tx_3 = Cagliari (39.2°N; 9.1°E), and Tx_4 = Catania (37.5°N; 15.1°E).

(3) The three grid points closest to each middle point with their corresponding $foF2_S$ and $M(3000)F2_S$ values are identified (green arrows of Fig. A2.1).
(4) $foF2_M$ and $M(3000)F2_M$ values at the middle points are calculated as the arithmetic average of the three values of $foF2_S$ and $M(3000)F2_S$ identified at point 3).
(5) The critical frequency of the E layer, foE_M, is calculated with Eq. (A1.7) for each middle point.
(6) The $MUF_{LKW}(D)F2$ is calculated with Eq. (A1.1) for each link (Tx_j-Rx_i).
(7) A graphical procedure is then applied to get the contour lines of the $MUF_{LKW}(D)F2$ and consequently the corresponding *skip distances*.

References

Belehaki, A., Cander, L.R., Zolesi, B., Bremer, J., Juren, C., Stanislawska, I., Dialetis, D., Hatzopoulos, M., 2005. DIAS Project: the establishment of a European digital upper atmosphere server. J. Atmos. Solar Terr. Phys. 67 (12), 1092–1099. https://doi.org/10.1016/j.jastp.2005.02.021.

Belehaki, A., Tsagouri, I., Kutiev, I., Marinov, P., Zolesi, B., Pietrella, M., Themelis, K., Elias, P., Tziotziou, K., 2015. The European Ionosonde Service: nowcasting and forecasting ionospheric conditions over Europe for the ESA Space Situational Awareness services. J. Space Weather Space Clim. 5, A25. https://doi.org/10.1051/swsc/2015026.

Bianchi, C., De Santis, A., Meloni, A., Zolesi, B., 1992. Magnetic and Ionospheric Effects of the Strong Magnetospheric Storm of March 13th, 1989 over Italy. Il Nuovo Cimento. 15 C, N. 1.

Bilitza, D., Reinisch, B.W., 2008. International Reference Ionosphere 2007: improvements and new parameters. Adv. Space Res. 42 (7), 599–609. https://doi.org/10.1016/j.asr.2007.07.048.

Bilitza, D., Altadill, D., Zhang, Y., Mertens, C., Truhlik, V., Richards, P., McKinnell, L.-A., Reinisch, B., 2014. The International Reference Ionosphere 2012 – a model of international collaboration. J. Space Weather Space Climate 4, A07. https://doi.org/10.1051/swsc/2014004.

Bilitza, D., Altadill, D., Truhlik, V., Shubin, V., Galkin, I., Reinisch, B., Huang, X., 2017. International Reference Ionosphere 2016: from ionospheric climate to real-time weather predictions. Space Weather 15 (2), 418–429. https://doi.org/10.1002/2016SW001593.

CCIR, 1991. Atlas of Ionospheric Characteristics, Comité Consultatif International des Radiocommunications Report 340–6. Int. Telecommun Union, Geneva.

Davies, K., 1990. "Ionospheric Radio" printed in England by Short Run Press Ltd., Exeter and published by Peter Peregrinus Ltd., London, United Kingdom.

Dominici, P., 1971. Radiopropagazione Ionosferica, Monografie Scientifiche e Tecniche del Servizio Ionosferico Nazionale.

Ezquer, R.G., Lopez, J.L., Scida, L.A., Cabrera, M.A., Zolesi, B., Bianchi, C., Pezzopane, M., Zuccheretti, E., Mosert, M., 2014. Behaviour of ionospheric magnitudes of F2 region over Tucuman during a deep solar minimum and comparison with the IRI 2012 model predictions. J. Atmos. Solar Terr. Phys. 107, 89–98. https://doi.org/10.1016/j.jastp.2013.11.010.

Galkin, I.A., Reinisch, B.W., 2008. The new ARTIST 5 for all Digisondes, in Ionosonde Network Advisory Group Bulletin. In: IPS Radio and Space Serv., Surry Hills, N. S. W., Australia, vol. 69, pp. 1–8. Available also at: http://www.ips.gov.au/IPSHosted/INAG/web-69/2008/artist5-inag.pdf.

Houminer, Z., Bennett, J.A., Dyson, P.L., 1993. Real-time ionospheric model updating. J. Electr. Electr. Eng., Austr., IE Austr. & IREE Austr. 13 (2), 99–104.

Lockwood, M., 1983. A simple M factor algorithm for improved estimation of the basic maximum frequency of radio waves reflected from the ionospheric F region. Proc. IEE, 130F, pp. 296–302.

McNamara, L., 1991. "The Ionosphere: Communications, Surveillance, and Direction Finding" printed and published by KriegerPublishing Company.

Perna, L., Pezzopane, M., Pietrella, M., Zolesi, B., Cander, L.R., 2017a. An updating of the SIRM model. Adv. Space Res. 60, 1249–1260. https://doi.org/10.1016/j.asr.2017.06.029.

Perna, L., Pezzopane, M., Ezquer, R., Cabrera, M., Baskaradas, J.A., 2017b. NmF2 trends at low and mid latitudes for the recent solar minima and comparison with IRI-2012 model. Adv. Space Res. 60, 363–374. https://doi.org/10.1016/j.asr.2016.09.025.

Pezzopane, M., Scotto, C., 2005. The INGV software for the automatic scaling of foF2 and MUF(3000)F2 from ionograms: a performance comparison with ARTIST 4.01 from Roma data. J. Atmos. Solar Terr. Phys. 67 (12), 1063–1073. https://doi.org/10.1016/j.jastp.2005.02.022.

Pezzopane, M., Scotto, C., 2007. The automatic scaling of critical frequency foF2 and MUF(3000)F2: a comparison between Autoscala and ARTIST 4.5 on Roma data. Radio Sci. 42, RS4003. https://doi.org/10.1029/2006RS003581.

Pietrella, M., 2015. A software package generating long term and near real time predictions of the critical frequencies of the F2 layer over Europe and its applications. Int. J. Geosci. 6 (4), 373–387. https://doi.org/10.4236/ijg.2015.64029.

Pietrella, M., Perrone, L., Fontana, G., Romano, V., Malagnini, A., Tutone, G., Zolesi, B., Cander, L.J.R., Belehaki, A., Tsagouri, I., Kouris, S.S., Vallianatos, F., Makris, J.P., Angling, M.J., 2009. Oblique-incidence ionospheric soundings over Central Europe and their application for testing now casting and long term prediction models. J. Adv. Space Res. 43 (11), 1611–1620. https://doi.org/10.1016/j.asr.2008.01.022.

Radicella, S.M., 2009. The NeQuick model genesis, uses and evolution. Ann. Geophys. 52 (3/4), 417–422.

Reinisch, B.W., Huang, X., 1983. Automatic calculation of electron density profiles from digital ionograms: 3. Processing of bottom side ionograms. Radio Sci. 18 (3), 477–492. https://doi.org/10.1029/RS018i003p00477.

Reinisch, B.W., Huang, X., Galkin, I.A., Paznukhov, V., Kozlov, A., 2005. Recent advances in real-time analysis of ionograms and ionospheric drift measurements with digisondes. J. Atmos. Solar Terr. Phys. 67 (12), 1054–1062. https://doi.org/10.1016/j.jastp. 2005.01.009.

Rishbeth, H., Garriot, O.K., 1969. Introduction to Ionospheric Physics. Academic Press, New York and London, p. 334.

Rishbeth, H., Muller-Wodarg, I.C.F., Zou, L., Fuller-Rowell, T.J., Millward, G.H., Moffett, R.J., Idenden, D.W., Aylward, A.D., 2000. Annual and semiannual variations in the ionospheric F2-layer: II. Physical discussion. Ann. Geophys. 18 (8), 945–956. https://doi.org/10.1007/s00585-000-0945-6.

Scotto, C., Pezzopane, M., 2002. A software for automatic scaling of foF2 and MUF(3000)F2 from ionograms. Proceedings of the XXVII General Assembly of the International Union of Radio Science, 17–24 August, Maastricht, The Netherlands. International Union of Radio Science, Ghent, CD-ROM.

Scotto, C., Pezzopane, M., 2008. Removing multiple reflections from the F2 layer to improve Autoscala performance. J. Atmos. Solar Terr. Phys. 70 (15), 1929–1934. https://doi.org/10.1016/j.jastp.2008.05.012.

Scotto, C., 2009. Electron Density profile calculation technique for Autoscala ionogram analysis. Adv. Space Res. 44, 756–766. https://doi.org/10.1016/j.asr.2009.04.037.

Scotto, C., Pezzopane, M., Zolesi, B., 2012. Estimating the vertical electron density profile from an ionogram: on the passage from true to virtual heights via the target function method. Radio Sci. 47, RS1007. https://doi.org/10.1029/2011RS004833.

Tsagouri, I., Zolesi, B., Belehaki, A., Cander, L.R., 2005. Evaluation of the performance of the real-time updated simplified ionospheric regional model for the European area. J. Atm. Sol. Terr. Phys. 67 (12), 1137–1146. https://doi.org/10.1016/j.jastp.2005.01.012.

Tsagouri, I., Belehaki, A., 2008. An upgrade of the solar-wind-driven empirical model for the middle latitude ionospheric storm-time response. J. Atmos. Solar Terr. Phys. 70, 2061–2076. https://doi.org/10.1016/j.jastp.2008.09.010.

Tsagouri, I., Koutroumbas, K., Belehaki, A., 2009. Ionospheric foF2 forecast over Europe based on an autoregressive modeling technique driven by solar wind parameters. Radio Sci. 44, RS0A35. https://doi.org/10.1029/2008RS004112.

Zolesi, B., Cander, L.R., De Franceschi, G., 1993. Simplified ionospheric regional model for telecommunication applications. Radio Sci. 28 (4), 603–612. https://doi.org/10.1029/93RS00276.

Zolesi, B., Cander, L.R., De Franceschi, G., 1996. On the potential applicability of the simplified ionospheric regional model to different mid-latitude areas. Radio Sci. 31 (3), 547–552. https://doi.org/10.1029/95RS03817.

Zolesi, B., Belehaki, A., Tsagouri, I., Cander, L.R., 2004. Real-time updating of the simplified ionospheric regional model for operational applications. Radio Sci. 39 (2), RS2011. https://doi.org/10.1029/2003RS002936.

Zolesi, B., Fontana, G., Perrone, L., Pietrella, M., Romano, V., Tutone, G., Belehaki, A., Tsagouri, I., Kouris, S.S., Vallianatos, F., Makris, J. P., Angling, M.J., 2008. A new campaign for oblique-incidence ionospheric sounding over Europe and its data application. J. Atmos. Solar Terr. Phys. 70 (6), 854–865. https://doi.org/10.1016/j.jastp.2007.02.015.